Materials Advances

ROYAL SOCIETY OF CHEMISTRY

PAPER

View Article Online
View Journal | View Issue

Cite this: *Mater. Adv.*, 2024, 5, 9359

Characterization and assessment of cleaning systems based on fatty acid methyl esters (FAMEs) for the removal of wax-based coatings from cultural heritage objects†

Chiara Biribicchi, *[ab] Michael Doutre‡[c] and Gabriele Favero [d]

Received 2nd August 2024,
Accepted 25th October 2024

DOI: 10.1039/d4ma00781f

rsc.li/materials-advances

This study focuses on the characterization of fatty acid methyl esters (FAMEs) and their implementation as solvents for removing beeswax and microcrystalline wax from cultural heritage materials, emphasizing their potential as sustainable alternatives to conventional solvents. FAMEs, derived from renewable sources through triglyceride transesterification, offer biodegradability and low toxicity. Additionally, the inclusion of an innovative aluminum stearate-based organogelator aims to regulate the evaporation rate of FAMEs, enhancing their application on artwork surfaces while minimizing their penetration into a substrate. Solubility tests, scanning XRF, spectrophotometry, SEM, FT-IR ATR, and contact angle measurements confirmed that all tested cleaning systems could remove up to 99% of beeswax and microcrystalline wax. Volume effectiveness calculations demonstrate that lower-polarity FAMEs, with reduced evaporation rates, require smaller solvent volumes. Restricting evaporation and solvent quantities enhances sustainability and reduces environmental and operator risks. However, adopting less volatile solvents necessitates novel application methodologies to mitigate their penetration and retention in porous artwork substrates. This research underscores FAMEs' potential not only as solvent alternatives but also as promoters of sustainable conservation practices.

Introduction

Green Chemistry represents a fundamental tool to address the modern challenge of sustainable development. Periodic re-examination and redesign of processes and materials involved in producing, transforming, and utilizing chemical products play a key role in waste and harm minimization while maintaining or increasing efficiency.[1] Mitigation of the adverse consequences derived from substances produced and used by mankind constitutes one of the main sustainability goals, dictating to deal with threats posed by toxicity to the welfare of all living things.[2]

Moving in this direction, it is important to increase the people's understanding of sustainability and Green Chemistry as complex and multifaceted concepts requiring adequate dissemination to avoid misinformation.[3,4] Business, regulatory, and consumer interests generate pressure in defining particular chemicals or products as green or not green, but rigid categorization can be easily misleading for multiple reasons: (a) green criteria may vary based on the end use; (b) continuous improvement is always necessary; (c) substances that have not undergone thorough toxicological assessment are often sold or promoted as greener alternatives even though further studies are needed.[5]

It is of utmost importance to emphasize this concept among professionals in cultural heritage conservation, who should make consulting toxicological properties – through regulatory bodies like the European Chemical Agency (ECHA) or the Environmental Protection Agency (EPA) – a standard practice to prevent the development of long-term health issues.[6–12] Indeed, restorers are often subject to inhalation of solvent vapors while conducting conservation interventions, as cleaning treatments are primarily carried out using substantial quantities of solvents, often applied as free solvents by using and rubbing cotton swabs on the surface. Even though awareness on the risks that chemical products might pose is

[a] *Department of Earth Sciences, Sapienza University of Rome, P.le Aldo Moro 5, 00185 Rome, Italy. E-mail: chiara.biribicchi@uniroma1.it*
[b] *UCLA/Getty Interdepartmental Program in the Conservation of Cultural Heritage, University of California, A210 Fowler Building/Box 951510, 308 Charles E. Young Dr North, Los Angeles, CA 90095, USA*
[c] *Getty Conservation Institute (GCI), 1200 Getty Center Drive, Suite 700, Los Angeles, CA 90049, USA. E-mail: michael.doutre@pc.gc.ca*
[d] *Department of Environmental Biology, Sapienza University of Rome, Piazzale Aldo Moro 5, 00185 Rome, Italy. E-mail: gabriele.favero@uniroma1.it*

† Electronic supplementary information (ESI) available. See DOI: https://doi.org/10.1039/d4ma00781f

‡ Present address: Cultural Heritage Directorate, Parks Canada, Government of Canada, 1800 Walkley Rd, Ottawa, ON K1H 8K3, Canada.

continuously growing, high compatibility with the materials of artifacts still represents the leading feature for the selection of either traditional or new chemicals, often outweighing environmental and health concerns.[13] This is compounded by practical and economic reasons that limit the feasibility of engineering controls (such as fume extraction) to mitigate these concerns for many conservation professionals.

Solvents having medium–high evaporation rates are often preferred to reduce interaction between the cleaning agent and the constituent materials, thus possible damage in both the short and long terms. However, a high evaporation rate also implies higher dispersion of the solvent in the environment.[14]

In an attempt to replace harmful substances that are still widely used in the sector, many newly developed products have been introduced as ''green'' solutions. However, most of these should be more accurately considered ''greener'' alternatives to the more toxic options currently available, aimed at reducing or eliminating primary and secondary products that pose risks to human health and the environment.[15–26] Recent studies on Green conservation have been exploring bio-based or low-toxic solvents and methods involving the use of ionic liquids, deep eutectic solvents, supercritical fluids, microemulsions, micellar systems, and physical and chemical gels.[14,21,24,26–31] However, the development of greener cleaning systems for cultural heritage conservation is still an open topic, as these innovative methods must comply with the artifacts' original materials avoiding any kind of undesired alteration.[17] In addition, the majority of newly developed cleaning systems are intended to remove medium-to-high polar substances, while the removal of low-to-nonpolar substances has been achieved mostly with the implementation of composite systems such as chemical gels, inorganic emulsions, micellar solutions, and silicone-based systems.[25,32–38] While these composite systems are constantly gaining more attention as viable sustainable options for cleaning treatments, not many studies are focusing on the replacement of toxic low-polar solvents with greener ones.[18–20,24,39]

Fatty acid methyl esters (FAMEs) have been garnering increasing attention as greener fuel alternatives to petroleum diesel due to their biocompatibility and low-toxic nature.[40] FAMEs are produced *via* transesterification of triglycerides from recyclable and sustainable feedstocks such as vegetable oils or crude sources with methanol or ethanol as a solvent in the presence of a catalyst.[41–44] Their use reveals advantages due to their lower dependence on restricted resources, lower pollution, biodegradability, and renewability.[41] However, there are non-fuel uses for FAMEs, showing applications as solvents, lubricants, feedstock chemicals, and more.[40,45] These remarkable properties fostered the study of their performances as alternative solvents for the removal of low-polar substances from cultural heritage materials.

Natural and microcrystalline waxes have been extensively used as low-polar coatings to protect metal and stone artifacts from corrosion and erosion caused by weather, rain, and both primary and secondary atmospheric pollutants such as CO_2, SO_x, NO_x, and chlorides.[24,46–48] The low vapor permeability of waxes helps prevent corrosion processes on outdoor metal sculptures and growth of salt crystals within stone pores being driven or aggravated by precipitation, condensation and the washing effect of rainwater.[49–55] While beeswax was commonly used historically in restoration treatments for both protection and toning on metals and stones, nowadays, outdoor sculptures in these materials are mostly treated with microcrystalline wax.[46,47,53,56–60] For metal surfaces, acrylic coating is usually directly applied on the artifact before the application of the wax, which is used as a ''sacrificial layer'' intended to protect the acrylic layer from degradation by atmospheric pollutants and water.[61]

Structure defects, chemical alteration induced by weathering, and embedding of pollutants induced by low melting points cause the deterioration of these waxes.[46,48,51,52,62–64] Microcrystalline waxes have the tendency to become powdery and exfoliate after two to five years, necessitating periodic maintenance and cleaning treatments aimed at removing the deteriorated layer and applying a new protective coating.[49]

Solvents posing major hazards to human health and the environment still represent the preferred tool to achieve this goal. Aliphatic and aromatic hydrocarbons such as mineral spirits/white spirits and petroleum ethers are being extensively used as pure solvents or in mixtures due to their lack of inaction towards the artifact's original materials, medium–high evaporation rates – causing inhalation of high amounts of solvent vapor – low cost, transparency, and purity.[32,56,65–68] For this reason, this study aims at exploring the application of fatty acid methyl esters (FAMEs) in cleaning interventions on cultural heritage materials as a possible alternative to aliphatic and aromatic hydrocarbons. Due to their extensive use in conservation practice, beeswax and the microcrystalline wax R21 have been used as reference low-polar materials to be removed from stone and metal substrates.

In addition, aluminum stearate ($C_{54}H_{105}AlO_6$) has also been introduced as a new thickening agent for low-polar solvents and tested in combination with FAMEs to compensate for the solvents' low evaporation rate, thus controlling their release on the artwork's surface and penetration in the substrate porosity. Aluminum stearate is soluble in all types of solvents – including low-polar ones – and oils when heated to form permanent transparent and viscous solutions or gels.[69,70] Due to the limited use of thickening agents for low-polar solvents in the conservation sector, aluminum stearate has been explored as a gelling agent for low-polar substances.

Materials and methods

Selection of greener formulations and organogel preparation

Aiming at exploring the overall dissolution ability of FAMEs as a solvent class, five FAMEs with alkyl chains ranging from C6 to C18 were used. Based on their physico-chemical and toxicological properties, methyl hexanoate (MH, CAS no. 106-70-7), methyl octanoate (MO, CAS no. 111-11-5), methyl laurate (ML, CAS no. 111-82-0), methyl myristate (MM, CAS no. 124-10-7), and methyl oleate (MOL, CAS no. 112-62-9) were selected and purchased from Merck.

Table 1 Hansen solubility parameters (δ*D*, δ*P*, and δ*H*) with RED value, Teas fractional parameters (F_d, F_p, and F_h), boiling point (BP), and vapor pressure (VP)

Compound	ID	δ*D*	δ*P*	δ*H*	RED	F_d	F_p	F_h	BP (°C)	P° (kPa@25 °C)
Methyl hexanoate	MH	16	4.3	5.8	1.00	61.30	16.48	22.22	149.5	0.50
Methyl octanoate	MO	15.4	2.7	5.9	0.90	64.17	11.25	24.58	192.6	0.07
Methyl laurate	ML	16	2.1	5.2	0.77	68.67	9.01	22.32	262	5.5×10^{-4}
Methyl myristate	MM	16	1.9	4.2	0.63	72.40	8.60	19.00	323	6.5×10^{-5}
Methyl oleate	MOL	16.1	1.5	3.5	0.52	76.30	7.11	16.59	218	8.4×10^{-7}
Mixture	Mix	15.24	3.29	6.21	0.99	61.59	13.30	25.11	160.95	2.45
Mineral spirits	MS	15.8[74]	0.1[74]	0.2[74]	0.00	100.00	0.00	0.00	98	2.7

With respect to the physico-chemical properties, solubility parameters were evaluated through Hansen solubility parameters (HSPs) (Table 1).[71,72] Due to the lack of data on HSPs of beeswax and microcrystalline wax R21, the center of the sphere corresponds to the solvent that is most commonly used for the removal of these substances from artifacts, mineral spirits (MS). δ*D*, δ*P* and δ*H* are the parameters corresponding to dispersion, polar and hydrogen bonding forces, respectively, which were used to plot the solvents in the 3D graph and define the center of the sphere (Fig. 1a). A radius (R_0) of 7 has been chosen for the sphere amplitude. The solvents that fall within the Hansen sphere can be defined as "good solvents", thus potential candidates. The distance between the solvent and the solute is called R_a; the greater the R_a is, the less likely the solvent will have solubility comparable to the one of the reference solvent.[71] HSPs were then translated into Teas fractional parameters (commonly used in the cultural heritage conservation field) and plotted in the TEAS triangle, where F_d represents the dispersion force, F_p represents the polarity, and F_h represents hydrogen bonding (Fig. 1b).[73]

The physical state was also taken into consideration, and only solvents that are liquid at room temperature were considered. The selection was conducted according to the hazard classification provided by ECHA.[8]

In addition, a mixture (mix) of MO and another supposed greener, more polar solvents have been tested in order to achieve similar evaporation rates to MS.

The physico-chemical properties of solvents are reported in Table 1, including the Hansen solubility parameters (δ*D*, δ*P*, and δ*H*), relative energy difference (RED), Teas fractional parameters (F_d, F_p, and F_h), boiling point (BP), and vapor pressure (P°). The RED is defined as the ratio R_a/R_0, where values lower than 1 are associated with "good solvents".[71]

Aluminum stearate (Thermo Scientific Chemicals, CAS no. 637-12-7) was used as a thickening agent coupled with the non-ionic surfactant Ecosurf EH-9 (CAS no. 64366-70-7) and mixed with one FAMEs to assess eventual differences between the pure solvent and the gelled one in selective removal, solvent release, residues left, and the amount of solvent used.

The final relative proportions of the constituents were determined after experimental testing, considering different concentrations of the surfactant and the thickening agent. Specifically, 12 ml of MM and 1 g of Ecosurf EH-9 were combined with 0.8 g of aluminum stearate (AS), placed in a closed vial, and heated to 85 °C under magnetic stirring until gelation occurred. The organogel (OG) was then allowed to equilibrate at room temperature and used for cleaning tests.

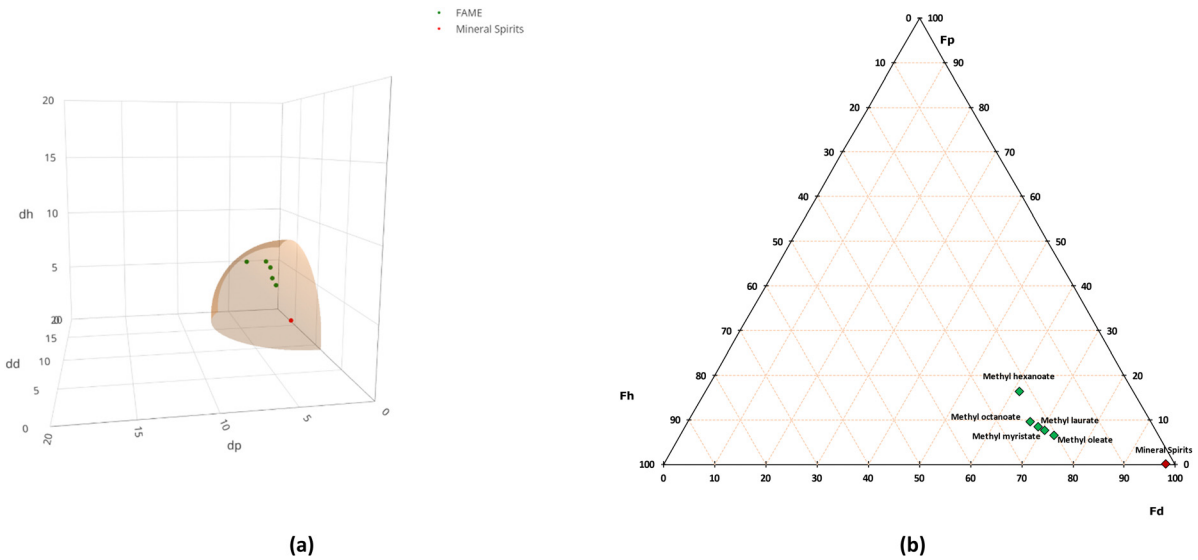

Fig. 1 (a) The Hansen sphere showing FAMEs' and mineral spirit parameters. (b) Teas triangle showing FAMEs' and mineral spirit fractional parameters.

FAMEs and organogel characterization through FT-IR ATR

Fourier transform infrared spectroscopy in the attenuated total reflectance mode (FT-IR ATR) was employed to characterize the FAMEs and to confirm the presence of various constituents within the formed organogel. A Bruker Alpha II FT-IR spectrometer equipped with a platinum ATR accessory and OPUS 5.0 software was used for acquisitions. A total of 24 scans were performed on each sample, with a resolution of 4 cm^{-1}, within the range of 4000–400 cm^{-1}.

Solubility tests

Solubility tests were conducted on both bleached beeswax and the microcrystalline wax R21 with each solvent by adding 0.1 g of the solute and 5 ml of the solvent into 10 ml glass vials. The closed vials were placed in a FS20 Fischer Scientific™ Ultrasonic Cleaner (90 W, 50–60 Hz) for five minutes and brought to ~20 °C to reach thermal equilibrium. Solutions were then filtered through an Advantec® PTFE filter (PF100, 47 mm) after imbibing it with ethanol to facilitate solvents flow through the filter and enhance the evaporation rate of low-volatile solvents. Each PTFE filter was weighted with an AY220 Shimadzu Corporation electronic balance (0.2 mg readability) before filtration and thirty days after filtration to drain low-volatile solvents. In addition, blank filters were poured in 5 ml of each solvent separately after imbibing them with ethanol. They were weighted both before imbibition and after solvent bath to understand the retention of the sole solvent in the filter. Eventual weight differences were subtracted from the weight difference between filters before and after pouring the solvent–wax solution to reduce solvent interference in gravimetric measurements.

Each measurement was repeated three times to reduce uncertainty. Results are reported as the percentage of wax dissolved relative to the total initial amount of wax present.

Contact angle measurements

Contact angle measurements were conducted with a Data Physics OCA 15 PRO Optical Tensiometer. Pure FAMEs and MS drops were applied on glass slides coated with both beeswax and R21 microcrystalline wax to observe waxes wettability and, consequently, their affinity with the solvents. MS and deionized water were used as nonpolar and polar reference materials, respectively. Each measurement was carried out ten times to reduce the uncertainty of the analysis.

Mock-up testing

Mock-up preparation. White Carrara marble and Roman travertine were purchased from a stone fabrication company in Los Angeles (CA), and bronze sheets (88% Cu, 12% Sn) were purchased from a local store. All samples were cut to 3.5 × 3.5 × 1.5 cm. Ten marble and ten travertine samples were covered with 1 ml of microcrystalline wax R21 in 20 wt% MS (CAS no. 64475-85-0, Spectrum® Chemical) loaded with 4 wt% cerium oxide (CeO_2, Gold Label). Ten marble and ten travertine samples were covered with 1 ml of bleached beeswax in 16.6 wt% mineral spirits (CAS no. 64475-85-0, Spectrum® Chemical) loaded with 4 wt% cerium oxide (Gold Label). As an intermediate acrylic layer is usually applied on outdoor metal artifacts before the application of the microcrystalline wax, 0.4 ml of Paraloid B72 (Kremer Pigmente GmbH & Co. KG) in 10 wt% acetone (CAS no. 67-64-1) was loaded with 2 wt% Cobalt Blue–Turquoise Dark (Cobalt Chrome Aluminate, $Co(Cr,Al)_2O_4$, Pigment Blue 36, CAS no. 68187-11-1; Kremer Pigmente GmbH & Co. KG) and applied on ten bronze samples. One week after the application of the acrylic layer, 0.5 ml of microcrystalline wax R21 in 20 wt% mineral spirits (CAS no. 64475-85-0, Spectrum® Chemical) loaded with 4 wt% cerium oxide (Gold Label) were applied.

Cerium oxide and cobalt blue were used as markers in order to make the coatings detectable using elemental and spectroscopic techniques and evaluate the effectiveness of the cleaning tests. The samples were analyzed before and after each coating layer was applied, as well as after the cleaning treatment, and then compared.

Mock-up cleaning. Cleaning tests were conducted using neat FAMEs and the mixture was applied with cotton swabs gently rolled over the sample surface to enhance dissolution while minimizing the mechanical pressure on wax removal. The duration of the treatment varied depending on the effectiveness and chemical–physical properties. The organogel was spread onto the surfaces of the mock-ups using a small spatula, with two layers of tengucho Japanese paper interposed to allow the solvent to gradually penetrate and release onto the target surface, minimizing the risk of leaving gel residues behind and aligning with common operational practices in cultural heritage conservation. The tengucho Japanese paper was also used to facilitate periodic observation of the treatment effects. By lifting the paper and gently rolling a cotton swab to remove the dissolved wax, it was possible to determine the optimal application times. Following the treatment with the organogel, any potential gel residues were not removed with a washing step to ensure that we could accurately observe the eventual presence of residues through FT-IR ATR analysis.

For neat solvents, the volume used was quantified to assess the environmental impact of the proposed solvents based on the amount required for the treatment. Solvents were placed in closed vials in predetermined quantities, which were only opened to immerse the swab before being closed again. The residual solvent was measured at the conclusion of the cleaning treatment. Concurrently, the time required for removal was recorded by measuring only the swabbing duration.

Technical photography: visible light (VL) and ultraviolet fluorescence (UVF). Photographic documentation in visible light (VL) and ultraviolet fluorescence (UVF) was used for the preliminary assessment of the presence of wax residues on the surface of samples. CeO_2 minimizes marble and travertine exhibiting fluorescence emission in UVF and, together with cobalt blue, can be easily detected on bronze samples in VL. Pictures were taken before and after the application of each coating and after the cleaning tests. Images in VL were acquired with a Z 7II Nikon digital camera equipped with a ZEISS T* UV filter, while a Peca #916 Visible Pass Filter and a LDP LLC

X-NiteCC1 filter were used in addition to the ZEISS T* UV filter to block UV light and IR light, so as to acquire the response in the visible part of the spectrum. Two Interfit Quartz Halogen 1000 lamps (AC 120 V, 60 Hz) were used for acquisitions in VL, while two Wildfire IronArc® UV Lmp-150S Lamps (AC 120–227 V, 50–60 Hz) were used for UVF. Images were elaborated with Adobe Bridge, ColorChecker Camera Calibration, and Adobe Photoshop.

Spectrophotometry. A CM-2600d spectrophotometer (Konica Minolta Sensing, Inc.) was used with an 8 mm aperture for spectrophotometric analysis before and after the application of each coating and after the cleaning tests. Data were acquired using the Color Data Software CM-S100w SpectraMagic NX (version 3.4) with a specular component included (SCI), then elaborated by using the CIELAB ΔE^*_{ab} [75] described as follows (eqn (1)):

$$\Delta E^*_{ab} = \sqrt{(\Delta L^*)^2+(\Delta a^*)^2+(\Delta b^*)^2} \quad (1)$$

where ΔE^*_{ab} is the total color difference, ΔL^* is the difference in lightness/darkness values (+ = lighter; − = darker), Δa^* is the difference on the red/green axis (+ = redder; − = greener), and Δb^* is the difference on the yellow/blue axis (+ = yellower; − = bluer).

Each analysis was performed three times at three different locations of the same sample to reduce uncertainty. The cleaning efficacy has been calculated as the percent return to the color of the blank sample, where $\Delta E^*_{blank,\ wax}$ is the CIELAB color difference between the blank and the wax-coated sample and $\Delta E^*_{blank,\ cleaned}$ is the CIELAB color difference between the blank and the cleaned samples (eqn (2)).[76]

$$\text{Cleaning efficacy } (\%) = \frac{\Delta E^*_{blank,\ wax} - \Delta E^*_{blank,\ cleaned}}{\Delta E^*_{b,w}} \quad (2)$$

For the bronze samples, the goal was to remove only the microcrystalline wax layer (R21) while preserving the underlying Paraloid B72 layer. For this reason, two key metrics were calculated: the percent return to the color of the blank sample, indicating the complete removal of both the wax and Paraloid B72 layers, and the percent return to the color of the Paraloid B72 layer, reflecting the selective removal of only the R21 wax layer.

Negative values indicating great color differences with the reference values were conventionally assigned 0% efficacy.

X-Ray fluorescence scanning (XRF). A Bruker M4 Tornado scanning micro-XRF spectrometer was used to map the elemental distribution of Ce and Co present as markers in the two waxes and Paraloid B72, respectively. The analysis was performed on samples before and after the application of each coating, as well as after the cleaning tests to examine the presence of CeO_2-loaded wax both on the sample surface and, as to stone samples, within the pores with a depth of analysis of 0.5 cm. The analysis was conducted in ''area'' mode, and the X-ray tube parameters were set at 50 kV/600 μA, a detector energy resolution of 40 keV/130 kcps, and a measuring time of 14.2 mm s^{-1} (1 cycle). A 3 × 3 cm area at the center of the sample was selected as the target analytical area to reduce eventual thickness unevenness due to wax accumulation on the edges. Each analysis was performed three times and the net counts of the relevant elements – *i.e.*, Ca and Ce for stone samples, Cu, Co, and Ce for bronze samples – were used to define the effectiveness of the cleaning tests. Student's *t*-test was used to verify that the difference between the Ca values – for stone samples – and between the Cu values – for bronze samples – was not statistically significant so as to use them as fixed parameters and compare Ce counts.

Scanning electron microscopy (SEM). SEM was carried out on bronze samples after the application of both the acrylic layer and the R21 to ensure that the acrylic layer and the wax layer do not merge during the application of the wax. For this reason, it is essential to verify that there is no interaction between the solvent in which the wax is dispersed (MS) and the Paraloid B72. Such verification was deemed necessary to evaluate the results of the cleaning tests because, if a fusion of the two layers is observed, it is no longer possible to assess the selectivity of the solvents in removing only the wax layer. The analysis was conducted on specimens prepared by applying a pre-defined amount of wax with a pipette, as well as on an additional mock-up where, after the application of the acrylic layer, the wax was applied with a brush. This approach was used to investigate the potential influence of the mechanical action on the fusion of the two layers. SEM analysis was conducted in variable pressure mode (VP = 30 Pa) with a GeminiSEM 300-71-20 scanning electron microscope (Carl Zeiss Microscopy Ltd) in combination with SmartSEM software (version 6.06). A SE2 detector (type II secondary electrons) was used with a beam electron high tension target (EHT) of 3.00 kV and a 7.500 μm aperture.

ImageJ. XRF maps of blank travertine samples were used to measure big pores sizes and correlate the results with the amount of residual wax detected with XRF analysis. Maps were elaborated using ImageJ 1.54g, converted into 8-bit images, and binarized. The area of large pores was calculated using image thresholding. Results were correlated with the amount of residual wax detected with XRF analysis to understand the influence of the pore distribution on differences in the amount of residual wax between travertine samples.

Fourier transform infrared spectroscopy in the attenuated total reflectance mode. FT-IR ATR was carried out on samples before and after the application of each coating and after the cleaning tests to assess the presence of residues related either to the acrylic coating – for bronze samples – wax or to the tested cleaning systems. IR spectra were collected using a Bruker Vertex 70 FT-IR spectrometer and OPUS 5.0 software. A total of 64 scans were performed on each sample with a resolution of 4 cm^{-1} using a RT-DLATGS detector, within the range of 4000–400 cm^{-1}.

Results

Solubility parameters and evaporation rates

As both the Hansen sphere in Fig. 1 and RED values suggest that the selected FAMEs possess suitable solubility parameters, becoming increasingly similar to reference values – the MS ones – as the carbon alkyl chain increases. However, it is worth

noting that as the alkyl chain grows, the vapor pressure decreases and the boiling point increases, meaning that the evaporation rate of the solvent becomes ever lower.

FAMEs and organogel characterization through FT-IR ATR

From the comparison of the spectra acquired for the various FAMEs, differences attributable to the molecular structure can be observed (Fig. 2). The peak at 3006 cm^{-1} corresponds to the medium C–H stretching of alkenes and is present only in the spectrum of MOL, which is the only proposed solvent with a double bond in its molecular structure. The relative intensities of the peaks in the region between 2956 and 2850 cm^{-1} are indicative of the chain length of the solvents.[77] Shorter chain FAMEs, such as MH, exhibit more pronounced peaks corresponding to the asymmetric and symmetric $-CH_3$ stretching at 2956 and 2874 cm^{-1}, respectively, as $-CH_3$ groups are more concentrated compared to $-CH_2$ groups. In contrast, the peaks associated with the asymmetric stretching at 2933 cm^{-1} and the symmetric stretching at 2850 cm^{-1} of $-CH_2$ groups increase in intensity with the solvent chain length. A similar trend is observed for the same reasons in the range between 1465 and 1376 cm^{-1}, where the peak at 1465 cm^{-1} corresponds to the $-CH_2$ bending of alkanes while the peaks at 1437 and 1376 cm^{-1} correspond to the C–H bending of the methyl group ($-CH_3$). Other characteristic peaks of FAMEs can be observed at 1745 cm^{-1} (C═O stretching of esters), 1365 cm^{-1} (medium –CH bending of alkanes), between 1250 and 1117 cm^{-1} (strong C–O stretching), between 879 and 862 cm^{-1} (strong –CH bending), and at 725 cm^{-1} (methylene rocking vibration in alkanes, observed only in long-chain alkanes).

By examining the spectrum of the organogel once equilibrated at room temperature, the predominant peaks corresponding to MM, which is present in greater quantities than the other components, can be observed (Fig. 3). The presence of these peaks demonstrates the entrapment of the solvent – acting as a cleaning agent – within the 3D network following preparation, indicating that it has not evaporated and can be released from the organogel during cleaning. Some of these peaks are also attributable to aluminum stearate and Ecosurf EH-9. However, the presence of aluminum stearate in the organogel is observable also through peaks at 1590 cm^{-1} (COO^- stretching attributable to the O^- on the polar head of the stearate) and the relative intensity of the peaks at 1470 cm^{-1} ($-CH_2$ bending, intense in stearate) and 1438 cm^{-1} (bending of the methyl group, less intense in stearate).[78] The presence of Ecosurf EH-9 within the organogel is confirmed by the peak at 1102 cm^{-1}, related to C–O stretching.

Organogel formation

The mixing of the constituents in the specified relative proportions resulted in the formation of a semi-transparent organogel, which remains physically stable when stored at room temperature (20 °C). This product exhibits a viscosity conducive to easy application to the target material, while minimizing infiltration into porous substrates – an essential requirement for its use as a cleaning agent in the conservation of cultural heritage. This outcome was achieved after a series of experimental trials aimed at optimizing the proportions of the different components.

Initial tests explored the gelation of the solvent using only aluminum stearate – a metallic complex consisting of aluminum ions and stearate ions – at varying concentrations. Depending on the solvent-to-aluminum stearate ratio, the mixture either failed to form gel, forming only a liquid solution, or resulted in a semi-solid paste composed of microcrystals suspended in liquid upon cooling, as noted in previous studies.[79] In the former case, the lack of gelation was attributed to an insufficient amount of gelling agents. In the latter, the semi-solid paste was attributed to the linear arrangement of the long saturated alkyl chains from both the gelling agent and the solvent, which interacted *via* weak intermolecular London dispersion and van der Waals forces, creating a tightly packed structure. This method of preparation, however, is unsuitable for applications requiring a free-flowing viscous liquid, and it

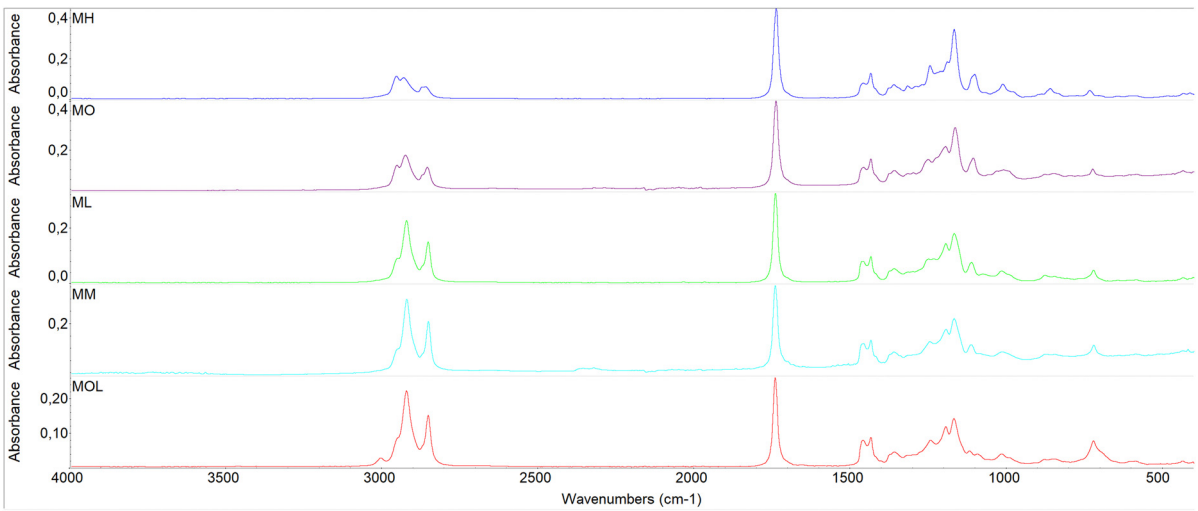

Fig. 2 FT-IR ATR spectra collected on FAMEs.

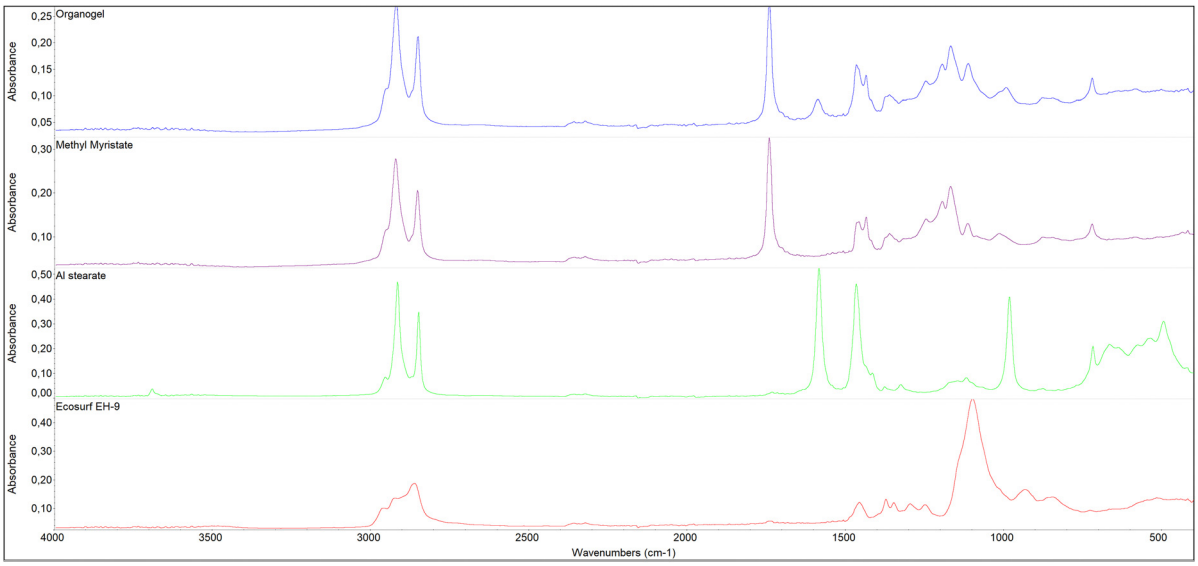

Fig. 3 FT-IR ATR spectra collected on the organogel and its raw components (MM, aluminum stearate, Ecosurf™ EH-9).

has been observed that the introduction of certain hydroxyl group (–OH)-containing substances can decrease the rigidity of the gel while simultaneously enhancing its viscosity.[79]

To increase the fluidity of the gel and disrupt its rigid structure, the surfactant Ecosurf EH-9 was added to the formulation. Ecosurf EH-9, an ethylene oxide-propylene oxide copolymer mono(2-ethylhexyl)ether, presumably acted by positioning itself between the interlaced structures, with its –OH end groups interacting with the carbonyl groups (–C═O) of both the aluminum stearate and methyl myristate (MM), thus relieving strain and tension within the gel matrix.[80] Indeed, the presence of polar groups effectively enhances interfacial tension between the nonpolar organic solvents and the gelator molecules, improving the overall fluidity of the system.[81]

Solubility tests

MO and MH showed in descending order the best results in terms of dissolution of beeswax, providing the lowest amount of wax residues (Table 2). Solubility tests conducted with ML, MM, and MOL resulted in the formation of a dispersion with beeswax, preventing the quantification of the wax residue alone. This result does not necessarily imply that ML, MM, and MOL have a lower ability to dissolve beeswax, but rather that their low evaporation rates enhance the retention of the solvents within the wax matrix, forming a dispersion where the low-volatility solvents become entrapped. Indeed, the final residue consists of both the wax and the solvent trapped within the wax matrix, resulting in a final weight exceeding that of the original wax used in the experiment (Table 2).

MH, MO, ML, and MM proved to have the greatest dissolution ability on the microcrystalline wax R21, in a descending order. A correlation between solvents' evaporation rate and the amount of residue wax can be noticed for the microcrystalline wax R21 as well, but of a lesser extent compared to beeswax. For the aforementioned reasons, the results of the solubility tests have to be interpreted taking into consideration the low evaporation rate of ML, MM, and MOL.

Table 2 Results of the solubility tests showing the percentage of wax dissolved relative to the total initial amount of wax present. S: maximum dissolution achieved, D: formation of a dispersion system consisting of both the wax and the solvent entrapped within it, U: undissolved, NM: not measurable because the weighted residue consists of the solvent–wax dispersion system

	Beeswax		R21	
Solvent	Result	Dissolved wax (%)	Result	Dissolved wax (%)
MH	S	57 ± 14	S	42 ± 1.4
MO	S	40 ± 1	S	38 ± 4.4
ML	D	NM	S	19 ± 2.1
MM	D	NM	S	14 ± 9.4
MOL	D	NM	D	NM
MS	U	NM	U	NM

Contact angle measurements

The measurements show the affinity of the FAMEs and the MS with the two waxes, justified by the low-polar properties of the solvents and the solutes, while water shows a very high contact angle due to the hydrophobicity of both waxes (Fig. 4). The R21 microcrystalline wax exhibits greater hydrophobicity compared to beeswax, presumably due to the presence of more polar components in the composition of beeswax.[82] Additionally, a progressive increase in the average contact angle value is observed as the chain length of the FAME increases. These differences may be partly due to a greater affinity of the solvents with the waxes, but also to the gradual, though slight, increase in the surface tension of the FAME as the chain length increases.[83,84]

Mock-up testing

Technical photography: visible light and ultraviolet fluorescence. Images in VL and UVF enabled the preliminary

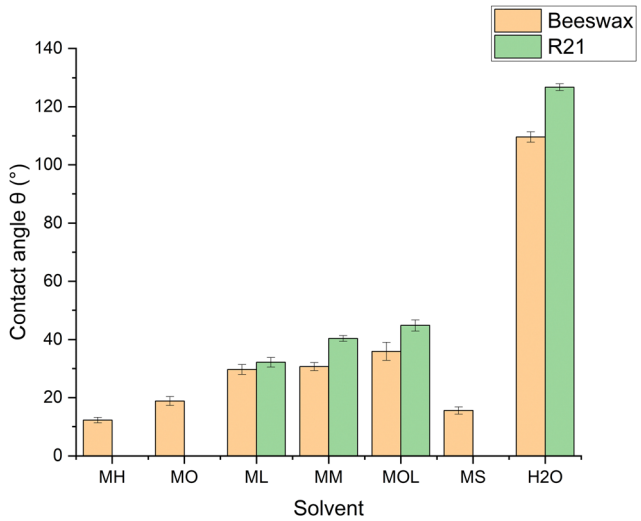

Fig. 4 Contact angle values measured by applying FAMEs on beeswax and R21 microcrystalline wax.

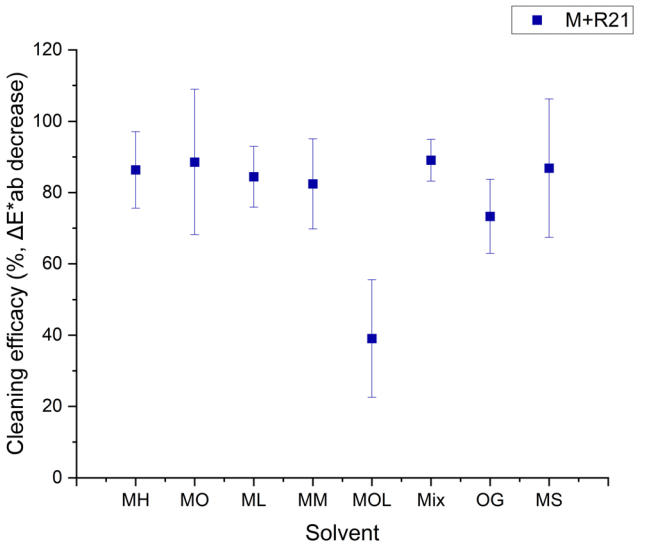

Fig. 5 Cleaning efficacy (%) on marble samples treated with microcrystalline wax R21 loaded with CeO, expressed as the percent return to the color of the blank sample. M: marble, R21: microcrystalline wax R21, mix: MO–polar solvent mixture, and OG: organogel.

assessment of the presence of wax residues on the sample surfaces (Tables S1–S5, ESI†). As stone samples, it is possible to observe how the fluorescence of the samples re-emerges after cleaning with all the solvents used, demonstrating that all of them were able to remove the wax layer present. At the same time, it can be noted that the fluorescence is less pronounced compared to that of the white samples, indicating that a certain amount of wax is still present within the pores. Regarding the bronze samples, it is evident that MH and MO have removed both the wax layer and the acrylic layer, due to their higher polarity. ML, on the other hand, caused the complete removal of the wax layer and partial solubilization of the Paraloid B72 layer, while MM and MOL, due to their lower polarity, allowed the acrylic layer to remain intact while removing the wax.

Spectrophotometry. Spectrophotometry was employed to assess whether the chromatic characteristics of the samples reverted to their reference values after the cleaning tests.[85] The higher the values of ΔE^*_{ab}, ΔL^*, Δa^*, and Δb^* obtained from the comparison between the cleaned and the reference values, the lower the cleaning efficiency.

Fig. 5–8 show the cleaning efficacy of the tested solvents in removing microcrystalline wax R21 and beeswax loaded with cerium oxide from the marble and travertine. It can be observed that all tested cleaning systems, with the exception of MOL, were able to remove between 73 ± 10% and 89 ± 6% of the R21 wax from the marble (Fig. 5). The tests conducted on R21-treated travertine produced different results, where shorter-chain FAMEs demonstrated lower efficacy (Fig. 6). This phenomenon can primarily be attributed to the inherent heterogeneity of the stone, which contains large pores into which the wax infiltrates, thus increasing the variability in colorimetric measurements, as reflected by the larger associated errors. For this reason, cleaning efficacy was predominantly assessed using marble specimens, as they present a more homogeneous surface.

A lower cleaning efficacy was observed in marble samples treated with beeswax, suggesting a more challenging removal process (Fig. 7). The highest efficacy was observed with MH, MO, ML, and OG, achieving removal rates between 39 ± 16% and 60 ± 12%. The persistent color alterations detected in the sample treated with MOL may be attributable to the saturation of the substrate due to the solvent's low evaporation rate. In contrast, the results obtained for travertine exhibited different behaviors, owing to the intrinsic heterogeneity of the substrate (Fig. 8).

In this case, no significant alterations were observed with MOL, and the cleaning efficacy was higher compared to marble samples, likely due to the infiltration of wax into the larger pores, resulting in a thinner layer of wax to be removed.

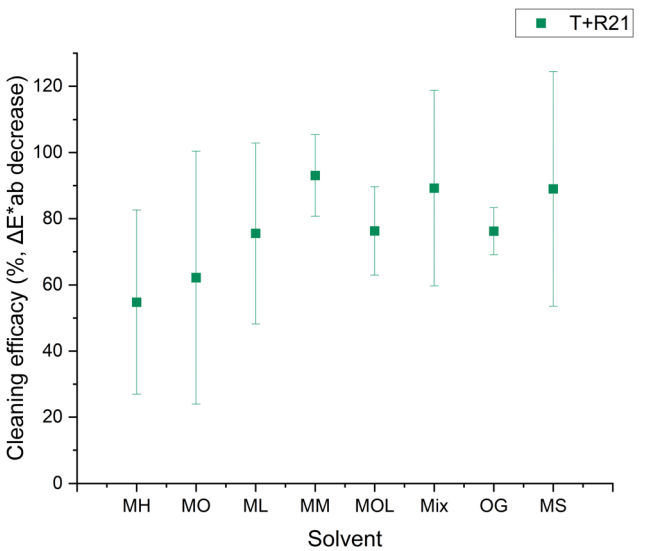

Fig. 6 Cleaning efficacy (%) on travertine samples treated with microcrystalline wax R21 loaded with CeO, expressed as the percent return to the color of the blank sample. T: travertine, R21: microcrystalline wax R21, mix: MO–polar solvent mixture, and OG: organogel.

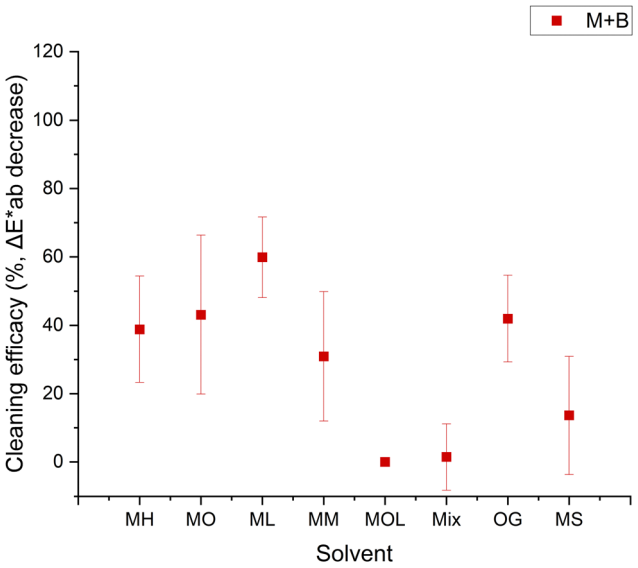

Fig. 7 Cleaning efficacy (%) on marble samples treated with beeswax loaded with CeO, expressed as the percent return to the color of the blank sample. M: marble, B: beeswax, mix: MO–polar solvent mixture, and OG: organogel.

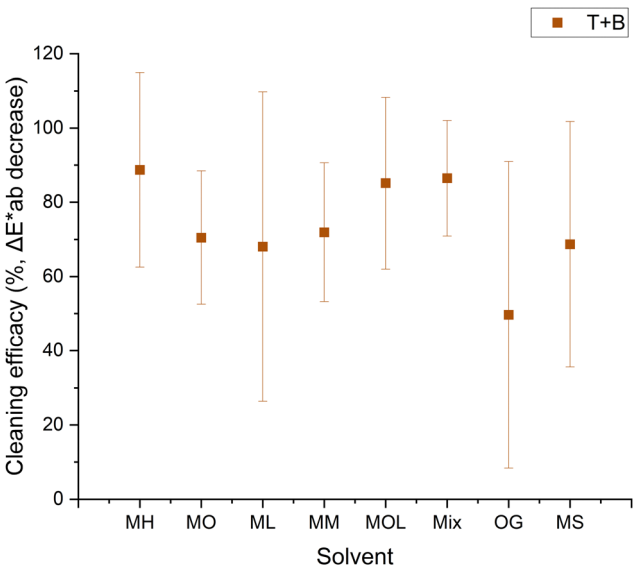

Fig. 8 Cleaning efficacy (%) on travertine samples treated with beeswax loaded with CeO, expressed as the percent return to the color of the blank sample. T: travertine, B: beeswax, mix: MO–polar solvent mixture, and OG: organogel.

Cleaning efficacy appeared more uniform across all solvents, although MOL, OG, and MS exhibited higher error margins, indicative of uneven removal.

For the bronze samples, Fig. 9 illustrates the cleaning efficacy of the tested systems in selectively removing the R21 wax layer while preserving the underlying Paraloid B72 layer, which contains cobalt blue pigment – this being the desired outcome. The figure also shows cases where both the wax and Paraloid B72 layers were removed, indicating that the cleaning

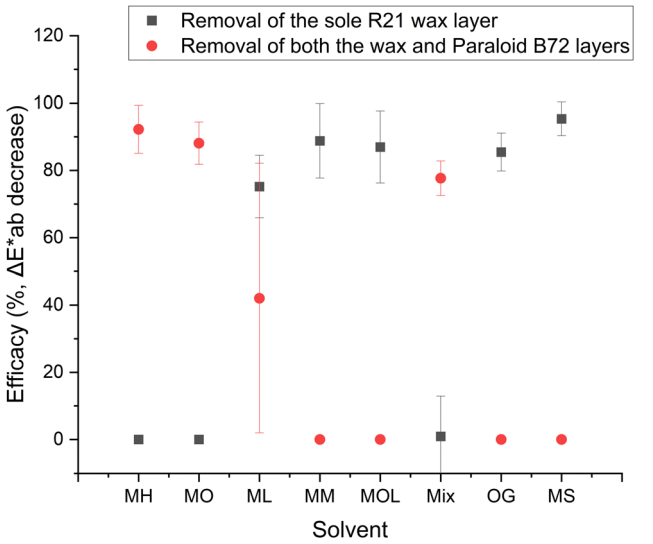

Fig. 9 Bronze samples treated with Paraloid B72 – loaded with cobalt blue – and the microcrystalline wax R21 – loaded with CeO. The efficacy (%) of cleaning systems is evaluated for the removal of the sole R21 wax layer, expressed as the percent return to the color of the Paraloid B72 layer, and for the removal of both the wax and Paraloid B72 layers, expressed as the percent return to the color of the blank sample. Mix: MO–polar solvent mixture and OG: organogel.

system interacted with the underlying acrylic layer, which was meant to be preserved. The two metrics exhibit inverse trends. In cases where both layers were removed using the cleaning system – such as with MH, MO, and mix – the efficacy for removing both layers ranged from 78 ± 5% to 92 ± 7%, while the efficacy for selectively removing only the wax was zero, as both layers were completely removed.

Conversely, for the other cleaning systems, the removal efficacy of both layers was zero, while the efficacy for removing only the wax ranged from 85 ± 6% to 95 ± 5%. The exception was ML, which partially affected the Paraloid B72 layer, resulting in an efficacy of 42 ± 40% for the removal of both layers. The high variability, indicated by the large error margin, is attributed to the uneven removal of the acrylic layer. These results demonstrate that MM, MOL, OG, and MS are capable of preserving the acrylic layer while effectively removing the overlying microcrystalline wax. This also suggests that the wax and acrylic layers do not merge during the application of the second layer, a hypothesis that will be further examined in the SEM analysis.

X-Ray fluorescence scanning. The XRF analysis provided data on element net counts, enabling a comparison of conditions before and after treatment. Simultaneously, the maps highlighted differences between the wax and the cerium oxide-coated sample and the sample post-treatment. Fig. 10 presents the normalized differences in Ce net counts in stone samples after cleaning with various solvents, compared to the Ce net counts in the waxes before treatment. The data clearly show that, despite variations in solvent effectiveness, all tested cleaning systems were able to remove approximately 82% to 99% of both beeswax and microcrystalline wax, demonstrating

the overall efficacy of the proposed solvents. However, the net Ce count in the treated travertine samples was higher than that in the treated marble samples. This is likely due to the larger pores in the travertine, which complicate the removal of wax with the cleaning method used. The XRF analysis, with its 0.5 cm resolution depth, reveals wax residues in the superficial layer of the samples. The generally lower effectiveness observed in the travertine samples treated with R21 wax can also be attributed to the wax's deeper penetration. This wax, due to its lower molecular weight compared to beeswax, more readily infiltrates the sample's structure.

To enhance result interpretation, the XRF maps obtained from the white samples were processed in ImageJ 1.54g, converted into 8-bit images, and binarized (Fig. 11a and b). The area of the largest pores was then calculated and correlated with the presence of residual cerium on the samples. The results show a positive correlation (p = 0.68 in the case of microcrystalline wax and p = 0.30 for beeswax), indicating that the pore sizes had an influence on the amount of detected cerium.

Due to inhomogeneity of travertine porosity, marble samples were given greater consideration to define the differences in the degree of cleaning among the different cleaning systems because their smoother surface provides a clearer indication of the cleaning effectiveness. It can be observed that all the FAMEs, except for MOL, were able to remove more than 98.6% of the applied beeswax and R21 wax (Fig. 10).

In the case of bronze samples, the analysis also allowed for the quantification of cobalt, indicating the residual amount of Paraloid B72 on the bronze surface post-wax removal. This highlights the solvent's ability to selectively remove the wax layer while preserving the integrity of the Paraloid B72 layer, in line with the objectives commonly pursued by conservators.

Upon examination, it can be observed that all cleaning systems were able to remove more than 98.7% of the applied R21 wax, further confirming the results of the investigations conducted on the stone samples and also demonstrating the MOL's ability to remove the protective layer similar to the other FAMEs when porosity is not a factor (Fig. 12). It is evident that the preservation of the acrylic layer was achieved primarily with less polar solvents – *i.e.*, MM, MOL, and MS – and the organogel, confirming previous analyses. Additionally, the dissolution ability of the organogel loaded with MM proves that the solvent is released by the 3D network and shows the same dissolution ability of the sole solvent while preserving the acrylic layer.

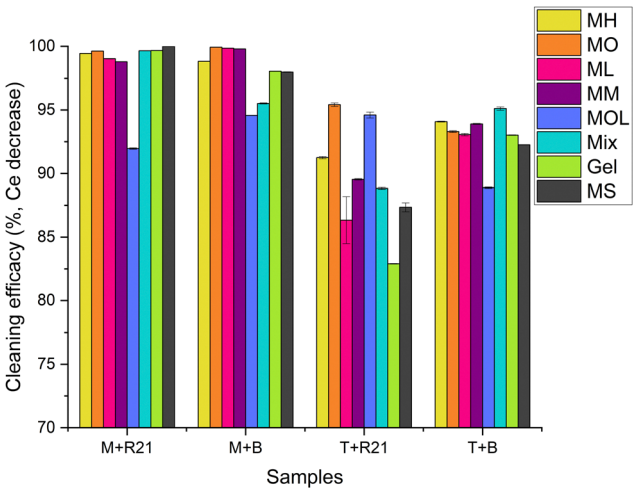

Fig. 10 Stone samples: normalized values of the removed wax calculated as the percentage difference in detected Ce between the cleaned samples and those coated with the waxes. M: marble, R21: microcrystalline wax R21, T: travertine, B: beeswax, mix: MO–polar solvent mixture, and OG: organogel.

Scanning electron microscopy (SEM). SEM acquisitions confirmed the successful separation of the microcrystalline wax layer from the acrylic layer, regardless of whether the wax was applied with a brush or a pipette (Fig. 13a and b).

It can thus be affirmed that, regardless of the introduction of mechanical action – such as the brushing motion used to apply wax dispersed in mineral spirits (MS) onto the acrylic layer on one of the two samples analyzed – the two layers do not tend to merge. Consequently, Paraloid B72 does not undergo even partial dissolution by the MS. This observation thus allows for the evaluation of the results obtained from the treatment of the bronze samples, especially concerning the ability to preserve the acrylic layer beneath the wax coating.

Fourier transform infrared spectroscopy in the attenuated total reflectance mode. FT-IR ATR was utilized to detect the presence of the organic components, specifically the two waxes and Paraloid B72, post-cleaning treatment, and to corroborate findings from elemental analysis techniques. In the analysis of stone samples, particular attention was given to the characteristic peaks of waxes at 2850 and 2920 cm^{-1}, indicative of C–H stretching in alkanes (Fig. 14). Considering that FT-IR ATR is a point-specific, predominantly qualitative technique, the acquisitions were not interpreted in quantitative terms. However, it is possible to observe that a wax residue was detected on all marble and travertine samples, regardless of the type of wax, validating the results of the XRF investigations – which identified residual Ce in all samples, albeit in reduced quantities – as well as spectrophotometric analyses and technical photography (Tables S6–S8, ESI†). Consequently, it is feasible to effectively correlate the presence of residual Ce with the persistence of wax on the samples. It is important to note that the peaks at 2850 and 2920 cm^{-1} could also be associated with the presence of solvent residues on the surface, as these are the characteristic peaks of FAMEs. However, unlike microcrystalline wax R21, such solvents exhibit a distinct peak at 1736 cm^{-1}, corresponding to the stretching mode of the carbonyl group C═O, which is not present in the spectra acquired after the cleaning treatments.[86,87] Most of the peaks related to beeswax instead correspond to the characteristic peaks of FAMEs, which do not allow for a straightforward interpretation of the spectra. However, they exhibit a similar trend to that observed in samples treated with R21 wax, where solvents with lower evaporation rates were also not detected, likely due to their penetration into the pores.

A key observation is that no detectable stearate residues were observed on the sample surface using FT-IR spectroscopy. The characteristic peak at 1588 cm^{-1}, indicative of the

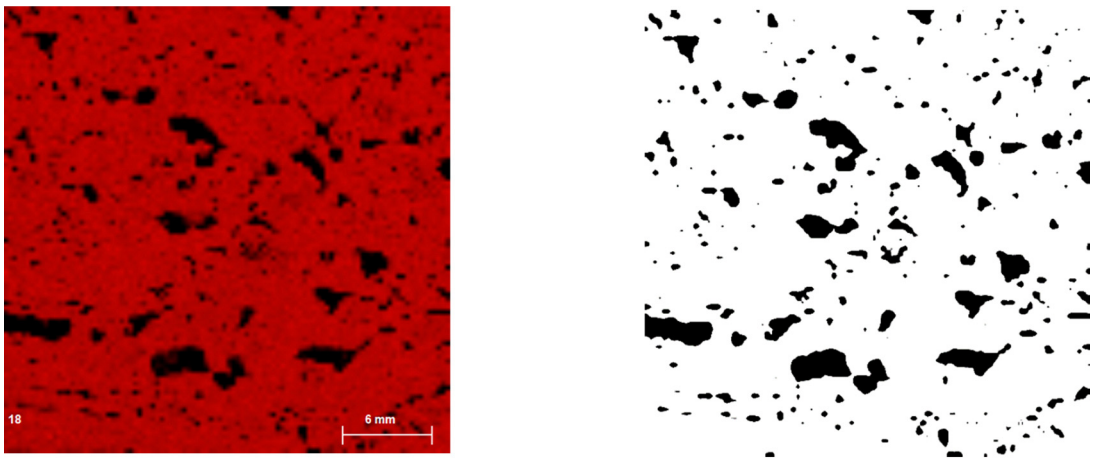

Fig. 11 (a) Example of an XRF map obtained from a white travertine sample and (b) a binarized map.

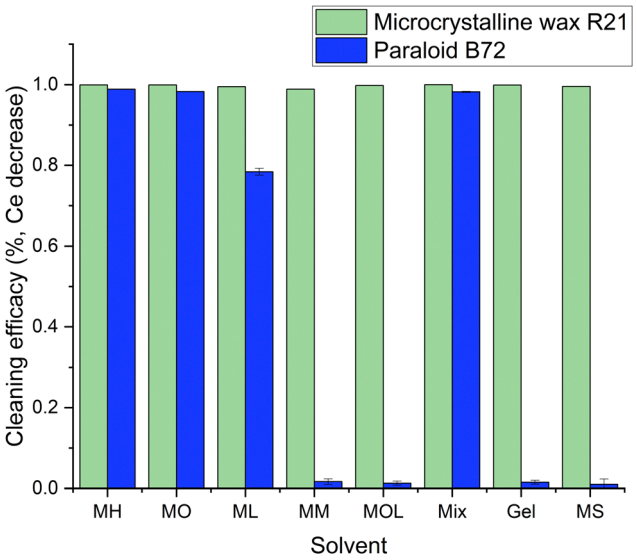

Fig. 12 Bronze samples: normalized values of the removed R21 wax calculated as the percentage difference in detected Ce between the cleaned samples and those coated with the wax, and the percentage difference in detected Co (corresponding to Paraloid B72) between the cleaned samples and those coated with the acrylic layer. Mix: MO–polar solvent mixture and OG: organogel.

asymmetrical stretching vibration of the COO^- group, was absent, suggesting that the organogel, when applied as described, does not leave residues detectable by FT-IR ATR on the treated surface (Fig. S1–S5, ESI†).[88]

Regarding the bronze samples, although the peaks at 2960, 2925, and 2870 cm^{-1} of Paraloid B72 may partially overlap with the characteristic peaks of wax, the spectra obtained allow for a clear distinction between the two materials. Moreover, Paraloid B72 is more easily identifiable due to its distinctive peaks at 1720, 1460, 1385, 1235, 1141, 1032, 966, and 745 cm^{-1}. The sample treated with methyl hexanoate (MH) exhibits faint peaks that correspond to the presence of residues of either wax or Paraloid, with these peaks being slightly more pronounced in the sample treated with methyl octanoate (MO) and the blend.

This suggests that both MH and MO effectively remove layers of both the acrylic and wax, leaving only slight residues indicative of the two protective materials. The longer chain solvents (ML, MM, and MOL) and mineral spirits (MS) also show more distinct peaks attributable to wax residues. Simultaneously, the prominent peaks of Paraloid B72 in these samples indicate the potential for preserving the acrylic layer when using longer chain solvents. The mixture yields results similar to those obtained with MH. Notably, the sample treated with the organogel demonstrates more prominent peaks associated with Paraloid B72, while the peaks related to wax are less evident, confirming the organogel ability to selectively remove the wax layer.

Volume of solvent used and time required for the tests. During the cleaning tests, both the amount of the solvent used to remove the wax layer and the time required for removal were quantified. An observable trend emerged for microcrystalline wax and beeswax, influenced by various factors. The interaction between solvents and solutes plays a crucial role in dissolution efficiency, affecting both the speed of coating removal and the quantity of the solvent required. However, this is balanced by the solvent's evaporation rate; higher evaporation rates lead to greater solvent dispersion into the environment, necessitating larger quantities for complete cleaning.

It can be observed that the volume required for the removal of microcrystalline wax increases with the polarity of the solvents (Fig. 15). This is due to the lower compatibility of more polar solvents with the non-polar microcrystalline wax. However, it is interesting to note that MOL (low volatility solvent) requires even less solvents than MS (reference solvent). Given its extremely low volatility, MOL, as well as ML and MM, although to a lesser extent, does not evaporate and remains on the surface to be treated for longer periods compared to more

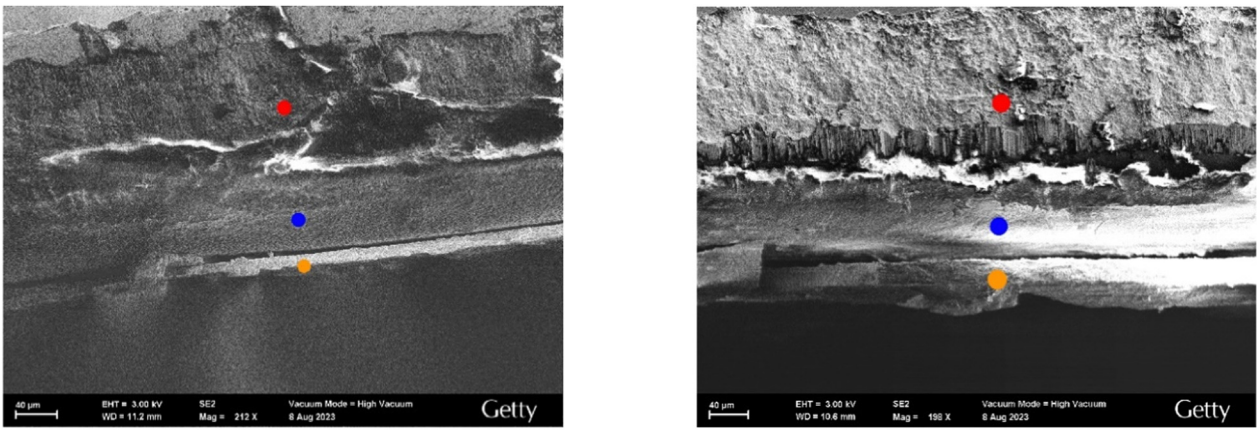

(a) (b)

Fig. 13 Cross-section of bronze samples treated with Paraloid B72 and the microcrystalline wax R21: (a) application using a brush and (b) application using a pipette. Red point: bronze sheet, blue point: Paraloid B72, and yellow point: microcrystalline wax R21.

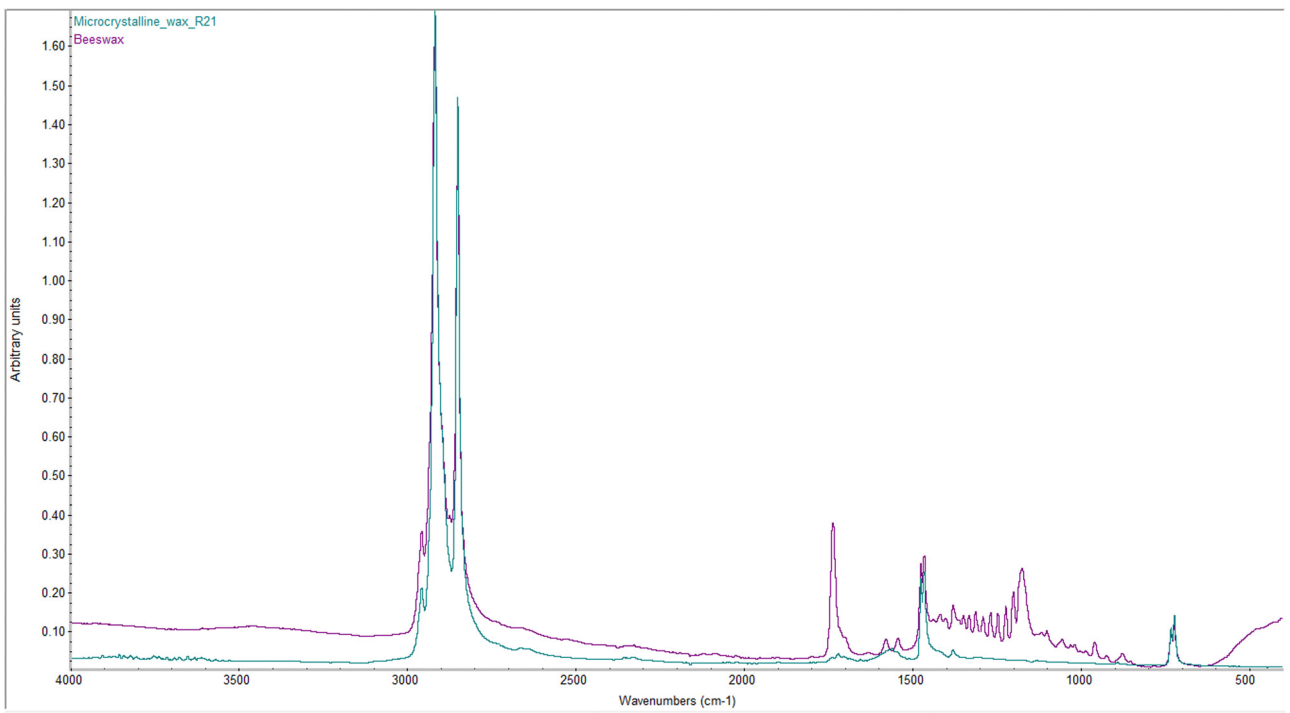

Fig. 14 FT-IR ATR spectra of beeswax and the microcrystalline wax R21.

volatile FAMEs. This factor allows for the use of reduced quantities of the product, with effectiveness similar to that of MS. At the same time, less volatile solvents like ML, MM, and MOL generally require shorter removal times compared to more volatile FAME solvents such as MH and MO (Fig. 16). For beeswax, the trend is somewhat different, as more polar solvents interact more significantly with the wax due to the presence of more polar functional groups in the beeswax compared to those in the microcrystalline wax. Nonetheless, in this case as well, MOL requires smaller quantities of solvents and shorter removal times – similar to MO and ML – compared to the more toxic reference solvent (MS) (Fig. 16 and 17).

Cultural heritage professionals often prefer to use solvents with a medium to high evaporation rate to minimize the interaction time with the materials of the artwork and to mitigate the risk of excessive solvent penetration. However, reducing the evaporation rate leads to lower dispersion of the substance into the environment and decreases the amount of solvent required, resulting in health, environmental, and potentially economic benefits.

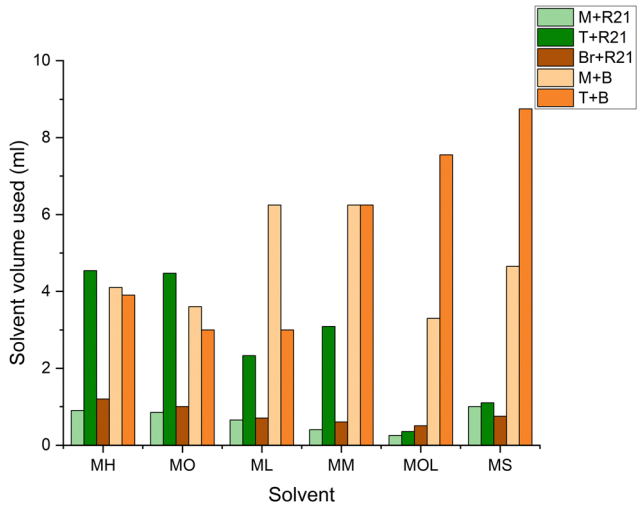

Fig. 15 Solvent volume used (ml) for the removal of the wax layer from the marble, travertine and bronze samples. M: marble, T: travertine, Br: bronze, R21: microcrystalline wax R21, and B: beeswax.

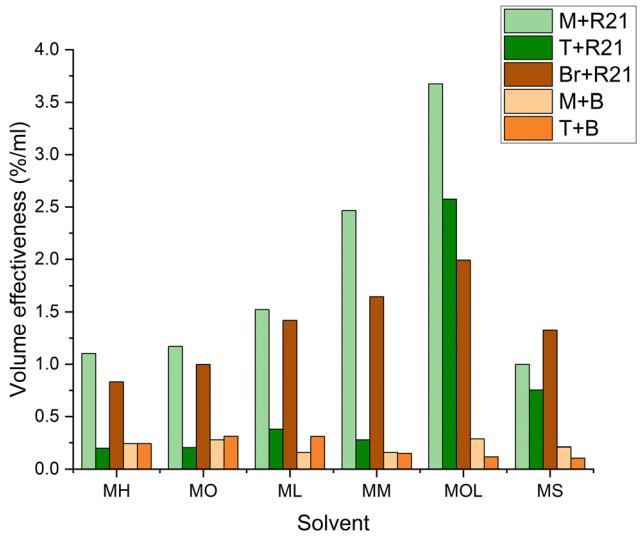

Fig. 17 Volume effectiveness: the ratio between the removed wax (in percentage) and the volume of the solvent used. M: marble, T: travertine, Br: bronze, R21: microcrystalline wax R21, and B: beeswax.

Discussion

This study evaluated the efficacy and sustainability of fatty acid methyl esters (FAMEs) as potential alternatives to conventional solvents in the removal of wax coatings from stone and metal artifacts. The findings highlight the significant potential of FAMEs, especially in terms of solubility performance and reduced health and environmental impacts.

The solubility tests revealed that MO and MH appeared to be particularly effective in dissolving beeswax, even though the partial entrapment of the solvent within the wax matrix complicates the interpretation of solubility efficiency for beeswax. However, it is possible to observe how shorter-chain solvents like MH and MO are particularly effective in dissolving not only beeswax, where the effectiveness of more polar solvents can be explained by the presence of various polar compounds in the wax composition, but also the microcrystalline wax R21, which is exclusively composed of hydrocarbons and therefore non-polar. Indeed, MO, ML, and MH were found to be particularly effective on the dissolution of the microcrystalline wax R21. This phenomenon can be explained by considering that smaller molecules have a greater solvent power, partially independent of solubility parameters. Indeed, the molecular size of both solvents and solutes plays a crucial role in phenomena such as solubility, permeation, diffusion, and chemical resistance. Both the Hildebrand solubility parameter theory and the Flory–Huggins theory of polymer solutions highlight that solvents with smaller molar volumes tend to be more effective than those with larger molar volumes, even when they have identical solubility parameters.[89,90] Currently employed solubility parameters for solvent selection – *i.e.*, Hildebrand and Hansen solubility parameters – do not comprehensively consider this factor. Indeed, efforts to incorporate a molecular volume into a composite solubility parameter and a size parameter have not yielded significant success. This may be because the impact of the molecular size is often more related to kinetic factors such as diffusion rates or considerations of free volume, rather than the thermodynamic principles that typically underpin solubility parameters.[89] However, this factor must be taken into consideration particularly in the field of cultural heritage conservation, where solubility parameters are the predominant tool, in combination with practical tests, for selecting solvents for artwork cleaning. Although solubility parameters are indispensable for solvent selection, considering molecular sizes could broaden the range of solvents to choose from, potentially paving the way for the use of even greener cleaning systems.

XRF analysis indicates that all tested cleaning systems, including FAMEs, are capable of removing between 82% and 99% of beeswax and microcrystalline wax. The higher net cerium (Ce) count in travertine samples post-treatment suggests

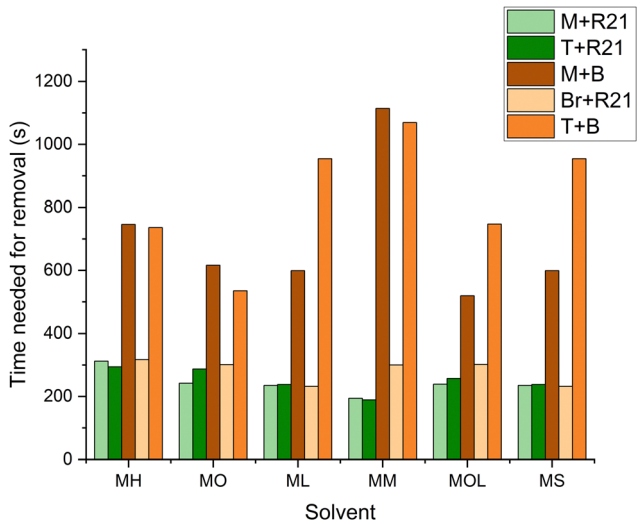

Fig. 16 Time (s) required for the removal of the wax layer from the marble, travertine and bronze samples. M: marble, T: travertine, Br: bronze, R21: microcrystalline wax R21, and B: beeswax.

that larger pores in travertine hinder complete wax removal, leading to the presence of residual wax. This observation indicated that while FAMEs are effective, their performance may vary based on the substrate's porosity. Nonetheless, all FAMEs except MOL achieved more than 98.6% removal of both beeswax and microcrystalline wax, demonstrating their high efficacy in various substrates. This is corroborated by the high removal efficiency (>98.7%) of all cleaning systems on bronze samples, underscoring the suitability of FAMEs in cleaning low-porosity surfaces.

The trend observed in the solubility tests conducted on microcrystalline wax R21 aligns with the XRF analyses carried out on the marble coated with microcrystalline wax. Given the uniform porosity of the marble and the consistency in the results from the solubility tests on R21 wax and the spectrophotometric analysis on the marble coated with R21, it is feasible to consider these data to assert that MH, MO, ML, and MM are the most effective solvents for the removal of microcrystalline wax.

As a general remark, MOL induced the most significant chromatic changes on marble, possibly due to solvent penetration that, even after a prolonged period, did not evaporate and increased the saturation of the sample. This phenomenon is not observed in travertine, likely because the solvent penetrated deeper due to the presence of larger pores, nor in bronze, due to the absence of porosity.

Based on the XRF and spectrophotometric analyses, as well as the solubility tests (though the latter are challenging to interpret due to the retention of less volatile solvents by the wax), beeswax appears to be slightly more soluble in the more polar FAMEs (MH, MO, and ML) compared to microcrystalline wax, despite also showing good solubility in the more non-polar FAMEs.

The observed differences between beeswax and microcrystalline wax can be attributed to their distinct compositions. Beeswax is composed of hydrocarbons (12–16%) with a predominant chain length of C27–C33, free fatty acids (12–14%) with chain lengths of C24–C32, linear wax monoesters and hydroxy monoesters (35–45%) typically ranging from C40 to C48, and complex wax esters (15–27%) and exogenous substances.[24,91] The broad solubility of beeswax in low- and medium-polar solvents can be attributed to the presence of long alkyl chains as well as more polar moieties, including –OH, –COOR′, and –COOH groups.[92] Furthermore, the fatty acid esters within beeswax contribute to a strong compatibility with the tested FAMEs. The carboxylic group –C═O of the FAMEs form hydrogen bonds with the hydroxy monoesters present in beeswax. Additionally, London dispersion forces play a significant role in the final solubility, involving the hydrophobic chains of both the solvent and the solute. As the chain length of the FAMEs increases, these dispersion forces also strengthen. However, molecules with shorter alkyl chains possess a higher concentration of polar groups per unit volume, which more effectively enhance the solubility of beeswax through interactions with its polar components. This explains why shorter-chain FAMEs tend to be somewhat more effective, even if no significant variations in efficacy are observed.

In contrast, microcrystalline wax is characterized by isoparaffinic (branched) hydrocarbons and naphthenic hydrocarbons, which are solubilized *via* weak intermolecular forces. Notably, the linear chains of FAMEs likely interact with the linear chains of the wax, enhancing compatibility with FAMEs that have longer alkyl chains compared to beeswax.

On bronze samples, MM, MOL, and MS showed minimal chromatic variations compared to the Paraloid B72-covered samples, indicating that these solvents can remove microcrystalline wax while preserving the underlying acrylic layer. While each tested cleaning system was able to remove the wax layer, these results highlight the importance of solvent selection in preserving the aesthetic and structural integrity of protective coatings that are intended to be preserved. This interpretation of the results was made possible by SEM analyses, which demonstrated that, regardless of the application method of the two protective layers, the microcrystalline wax and Paraloid B72 do not merge during application. Therefore, they can be selectively removed individually by choosing the appropriate solvent.

In addition, the organogel based on MM demonstrates approximately the same solvent removal capabilities as the pure solvent, highlighting the organogel's ability to release the solvent once applied to the surface without leaving residues detectable by FT-IR ATR analyses. This finding is particularly significant because the gelation of organic solvents, especially non-polar ones, which are suitable for use as cleaning agents on cultural heritage materials, is notably complex. The identification of a gelling system with the same cleaning efficacy as the pure solvent allows for the removal of the material from the artwork's surface while preventing excessive solvent release, laying the groundwork for further studies that explore the entrapment of the solvent within the gel system, as well as the release rate. Additionally, gelation helps reduce the release of solvents into the environment, consequently minimizing operator inhalation and pollutant dispersion, factors that enhance the sustainability of the entire cleaning process. In the same manner, it can be observed that the use of less volatile solvents allows for the use of smaller quantities of product, as they are not dispersed into the environment. Examining the volume effectiveness of the solvents, defined as the ratio between the removed wax (in percentage) and the volume of the solvent used, a trend is evident where a decrease in solvent polarity and volatility corresponds to an increase in volume effectiveness (Fig. 15). This means that a smaller quantity of the solvent is required to remove the same amount of wax. This finding is particularly important for understanding the impact that more volatile solvents have on sustainable development and how the use of lower evaporation rate systems can offer significant benefits for operator health and the reduction of environmental pollutants. It is equally critical to emphasize that this discussion should be contextualized into the field of cultural heritage conservation, where intervention methods must always consider potential side effects on the artifact. Indeed, the use of low-volatility solvents is generally avoided to limit solvent penetration into the substrate of the artifacts and prevent possible interactions, both short and long terms, with the constituent materials of the artifact, which could lead to degradation over time, such as color alterations or chemical

reactions between materials. For this reason, despite MOL having good solvent properties and requiring a smaller volume compared to other solvents, it risks causing significant color alterations and remaining in the pores for prolonged periods. Given their low volatility, the same applies to ML and MM. Therefore, the application of these products as pure solvents on porous materials should be avoided and replaced with alternative application methods, such as trapping the solvents in organogel systems that allow for gradual release exclusively at the organogel–surface interface of the artifact.

Conclusions

This study highlights the potential of FAMEs as effective, more sustainable alternatives to conventional solvents for the removal of low-polarity wax coatings from cultural heritage materials. The findings highlight that FAMEs, particularly MO, MH, ML, and MM, are highly effective in the removal of both beeswax and the microcrystalline wax R21, with the added benefit of reduced environmental impact and lower health risks compared to traditional solvents. Specifically:

- All FAMEs are capable of removing both waxes. However, beeswax exhibits slightly higher solubility in more polar FAMEs compared to microcrystalline wax.
- MM and MOL are the only FAMEs capable of removing the R21 wax layer while preserving the acrylic one underneath.
- The MM-based organogel exhibits comparable wax removal capabilities to pure MM, being able to release the solvent without leaving residues detected by FT-IR ATR.
- Solvents composed of small-sized molecules are effective even on completely nonpolar materials, such as R21 wax, despite their polarity not closely matching that of the material being removed.
- Despite the benefit of using less volatile solvents in smaller quantities, reducing environmental and health impacts, their direct application on porous or absorbent artworks is unsuitable due to the risk of prolonged persistence in the substrate possibly inducing further degradation. Therefore, alternative application methods, such as gelling systems, are recommended for further study.

As a general remark, the ability of FAMEs to remove wax coatings while preserving the underlying materials makes them promising candidates for conservation applications, aligning with green chemistry principles and sustainability goals.

However, it is important to emphasize that sustainable development should be intended as a gradual and progressive process, also suggesting that personal protection equipment (PE) is always recommended, and a careful approach is needed, especially when dealing with new materials. Agencies such as the European Chemicals Agency (ECHA) and the Environmental Protection Agency (EPA) ensure that companies comply with the legislation, advancing the safe use of chemicals, but also provide the final user with information on the physico-chemical and toxicological properties of chemicals.[8,9] Studies on the toxicological properties of certain substances are often incomplete and verification of any missing information should be undertaken by conservation professionals when handling new materials, always bearing in mind that future research might uncover adverse consequences that were previously unknown.

Additionally, it is important to consider that the implications of solvent evaporation extend beyond cleaning efficacy. The environmental and health impacts of solvent use are critical considerations in conservation practices. Higher volatility solvents – such as MH and MO – while potentially more effective, could result in prolonged exposure for the operator and greater environmental persistence. Therefore, the selection of solvents for conservation tasks should balance effectiveness, safety for both the operator and the artwork, and environmental impact. The findings underscore the importance of considering both the solubility and volatility characteristics when assessing solvent effectiveness for conservation purposes. Future research should focus on the long-term effects of FAMEs on treated surfaces and the development of formulations to further optimize their application for conservation use. Although an initial step in this direction has been made through the development of the gelling system described in this article, further studies are needed to more thoroughly verify the presence of residues following cleaning – for instance, through the use of gas chromatography/mass spectrometry (GC/MS) – as well as the release rate of the solvent and the ability to effectively retain it exclusively at the contact interface. Furthermore, other metal stearates known to be less toxic than aluminum stearate, such as calcium stearate, should be evaluated for their gelling and release capabilities.

Finally, future research should also focus on investigating the interactions between FAMEs and various materials found in other types of artworks, such as oil and acrylic paintings. Potential interactions with specific binders, for instance, could limit the applicability of FAMEs in cleaning treatments for surfaces sensitive to these compounds.

Author contributions

Conceptualization: C. B. and M. D.; methodology: C. B. and M. D.; validation: C. B. and M. D.; formal analysis: C. B. and M. D.; investigation: C. B.; resources: M. D.; data curation: C. B. and M. D.; writing – original draft preparation: C. B.; writing – review and editing: C. B., M. D. and G. F.; visualization: C. B.; supervision: M. D. and G. F.; project administration: M. D. and G. F.; funding acquisition: C. B. and M. D.

Data availability

The data supporting this article have been included as part of the ESI.†

Conflicts of interest

There are no conflicts to declare.

Acknowledgements

This work was supported by the PON ''Ricerca e Innovazione'' 2014–2020 (PON R&I FSE-REACT EU) and Azione IV.5 ''Dottorati su tematiche Green''. The authors want to express their gratitude to YOuth in COnservation of CUltural Heritage (YOCOCU APS) for the knowledge their members shared, thereby contributing to the development of this study. The authors would also like to thank the Getty Conservation Institute for providing access to their laboratory equipment and for the assistance provided by Tom Learner, Head of Science at the Getty Conservation Institute, as well as researchers Herant Khanjian and David Carson. The authors are also grateful to the UCLA/Getty Interdepartmental Program in the Conservation of Cultural Heritage, especially Glenn Wharton, for the support received during the research, and to Gianluca Ciarleglio for his help with the contact angle measurements.

References

1 C. J. Li and P. T. Anastas, *Chem. Soc. Rev.*, 2012, **41**, 1413–1414.
2 I. T. Horváth and P. T. Anastas, *Chem. Rev.*, 2007, **107**, 2167–2168.
3 S. V. de Freitas Netto, M. F. F. Sobral, A. R. B. Ribeiro and G. R. da L. Soares, *Environ. Sci. Eur.*, 2020, 32.
4 M. A. Delmas and V. C. Burbano, *Calif. Manage. Rev.*, 2011, **54**, 64–87.
5 M. J. Mulvihill, E. S. Beach, J. B. Zimmerman and P. T. Anastas, *Annu. Rev. Environ. Resour.*, 2011, **36**, 271–293.
6 N. P. Cheremisinoff, *Condensed Encyclopedia of Polymer Engineering Terms*, Butterworth-Heinemann, Oxford, 2001, pp. 301–326.
7 D. R. Joshi and N. Adhikari, *J. Pharm. Res. Int.*, 2019, **28**, 1–18.
8 ECHA – European Chemical Agency, **https://echa.europa.eu/home**, (accessed 25 September 2023).
9 European Parliament and Council, *Regulation (EC) No 1907/2006 of the European Parliament and of the Council of 18 December 2006 concerning the Registration, Evaluation, Authorisation and Restriction of Chemicals (REACH), establishing a European Chemicals Agency*, 2006.
10 ECHA, Understanding CPL.
11 EPA, Summary of the Toxic Substances Control Act.
12 OSHA, Chemical hazards and toxic substances.
13 E. Balliana, G. Ricci, C. Pesce and E. Zendri, *Int. J. Conserv. Sci.*, 2016, **7**, 185–202.
14 P. Baglioni, D. Berti, M. Bonini, E. Carretti, L. Dei, E. Fratini and R. Giorgi, *Adv. Colloid Interface Sci.*, 2014, **205**, 361–371.
15 P. G. Jessop, *Green Chem.*, 2011, **13**, 1391–1398.
16 F. Di Turo and L. Medeghini, *Sustainability*, 2021, **13**, 3609.
17 D. Chelazzi and P. Baglioni, *Langmuir*, 2023, **39**, 10744–10755.
18 B. Cattaneo, M. Picollo, F. Cherubini and V. Marchiafava, *Colour Photography and Film: Sharing knowledge of analysis, preservation, conservation, migration of analogue and digital materials*, Gruppo del Colore – Associazione Italiana Colore, Milan, 2021, pp. 174–178.
19 S. Prati, G. Sciutto, F. Volpi, C. Rehorn, R. Vurro, B. Blümich, L. Mazzocchetti, L. Giorgini, C. Samorì, P. Galletti, E. Tagliavini and R. Mazzeo, *New J. Chem.*, 2019, **43**, 8229–8238.
20 R. Strangis, M. Francesco, L. Russa, A. Macchia, C. Biribicchi, G. Salatino, A. Arcudi and R. Mancuso, in *2023 IMEKO TC-4 International Conference on Metrology for Archaeology and Cultural Heritage*, IMEKO, Rome, 2023, p. 6.
21 Y. Jia, G. Sciutto, A. Botteon, C. Conti, M. L. Focarete, C. Gualandi, C. Samorì, S. Prati and R. Mazzeo, *J. Cult. Herit.*, 2021, **51**, 138–144.
22 A. Macchia, C. Biribicchi, P. Carnazza, S. Montorsi, N. Sangiorgi, G. Demasi, F. Prestileo, E. Cerafogli, I. A. Colasanti, H. Aureli, M. Zappelli, M. Ricca and M. F. La Russa, *Sustainability*, 2022, **14**, 3972.
23 A. Källbom, *Int. J. Archit. Heritage*, 2022, **16**, 1112–1129.
24 C. Biribicchi, A. Macchia, G. Favero, R. Strangis, B. Gabriele, R. Mancuso and M. F. La Russa, *New J. Chem.*, 2023, **47**, 5991–6000.
25 C. Biribicchi, L. Giuliani, A. Macchia and G. Favero, *Sustainability*, 2023, **15**, 16305.
26 C. C. Fernandes, R. Haghbakhsh, R. Marques, A. Paiva, L. Carlyle and A. R. C. Duarte, *ACS Sustainable Chem. Eng.*, 2021, **9**, 15451–15460.
27 D. Chelazzi, R. Giorgi and P. Baglioni, *Angew. Chem., Int. Ed.*, 2018, **57**, 7296–7303.
28 C. Croitoru and I. C. Roata, *Processes*, 2024, **12**, 341.
29 P. Irizar, O. Gomez-Laserna, G. Arana, J. M. Madariaga and I. Martínez-Arkarazo, *J. Cult. Herit.*, 2023, **64**, 12–22.
30 L. H. Shockey, *AIC Objects Specialty Group Postprints*, 2009, vol. 16, pp. 13–24.
31 Y. Jia, G. Sciutto, R. Mazzeo, C. Samorì, M. L. Focarete, S. Prati and C. Gualandi, *ACS Appl. Mater. Interfaces*, 2020, **12**, 39620–39629.
32 G. Cavallaro, S. Milioto and G. Lazzara, *Langmuir*, 2020, **36**, 3677–3689.
33 D. Stulik, D. Miller, H. Khanjian, N. Khandekar, R. Wolbers, J. Carlson and W. C. Petersen, *Solvent Gels for the Cleaning of Works of Art: The Residue Question*, Getty Publications, Los Angeles, 2004th edn, 2004.
34 R. Wolbers and C. Stavroudis, *Conservation of easel paintings*, 2012, pp. 500–523.
35 M. Baglioni, G. Poggi, G. Ciolli, E. Fratini, R. Giorgi and P. Baglioni, *Materials*, 2018, **11**, 1144.
36 B. Ormsby, M. Keefe, A. Phenix, E. Von Aderkas, T. Learner, C. Tucker and C. Kozak, *J. Am. Inst. Conserv.*, 2016, **55**, 12–31.
37 G. Lo Dico, F. Semilia, S. Milioto, F. Parisi, G. Cavallaro, G. Inguì, M. Makaremi, P. Pasbakhsh and G. Lazzara, *Appl. Sci.*, 2018, **8**, 1455.
38 C. Briffa, *Investigating the removal of permanent marker ink from historical parchment, using acetone and benzyl alcohol with Velvesil Plus Gel*, **https://www.westdean.ac.uk/blog/investigating-the-removal-of-permanent-marker-ink-from-historical-parchment-using-acetone-and-benzyl-alcohol-with-velvesil-plus-gel**, (accessed 19 July 2023).

39 L. M. Elattar, S. S. Darwish, M. Ali and U. M. Rashed, *Egypt. J. Chem.*, 2022, **65**, 475–486.
40 D. Karis, R. Cain, K. Young, A. Shand, T. Holm and E. Springer, *Biofuels, Bioprod. Biorefin.*, 2022, **16**, 1893–1908.
41 I. Ambat, V. Srivastava and M. Sillanpää, *Renewable Sustainable Energy Rev.*, 2018, **90**, 356–369.
42 N. García-Martínez, P. Andreo-Martínez, J. Quesada-Medina, A. P. de Los Ríos, A. Chica, R. Beneito-Ruiz and J. Carratalá-Abril, *Energy Convers. Manage.*, 2017, **131**, 99–108.
43 A. G. Alsultan, N. Asikin-Mijan, Z. Ibrahim, R. Yunus, S. Z. Razali, N. Mansir, A. Islam, S. Seenivasagam and Y. H. Taufiq-Yap, *Catalysts*, 2021, 11.
44 A. S. Belousov, A. L. Esipovich, E. A. Kanakov and K. V. Otopkova, *Sustainable Energy Fuels*, 2021, **5**, 4512–4545.
45 Y. M. Gonzalez, P. De Caro, S. Thiebaud-Roux and C. Lacaze-Dufaure, *J. Solution Chem.*, 2007, **36**, 437–446.
46 B. Barclay and C. Hett, *CGI Notes*, 2007.
47 D. Comelli, G. Valentini, R. Cubeddu and L. Toniolo, *Fluorescence Lifetime Imaging and Fourier Transform Infrared Spectroscopy of Michelangelo's David*, 2005, vol. 59.
48 T. J. Shedlosky, K. M. Stanek and G. Bierwagen, *AIC Objects Speciality Group Postprints*, 2000, vol. 320, pp. 452–9545.
49 L. Robbiola, C. Fiaud and S. Pennec, in *ICOM Committee for Conservation Tenth Triennal Meeting*, Washington DC, 1993, p. 911.
50 E. Vara Fabjan, T. Kosec, V. Kuhar and A. Legat, *Mater. Technol.*, 2011, **45**, 585–591.
51 O. Seung-Jun and W. Koang-Chul, *J. Korea Convergence Soc.*, 2018, **9**, 151–160.
52 O. Seung-Jun and W. Koang-Chul, *J. Conserv. Sci.*, 2017, **33**, 121–130.
53 M. Toro, T. Beentjes, I. Joosten, J. Bloser and L. Zycherman, in Metal 2019 – *Interim Meeting of the ICOM-CC Metals Working Group*, Neuchatel, 2019.
54 B. Salvadori, D. Pinna and S. Porcinai, *Environ. Sci. Pollut. Res.*, 2014, **21**, 1884–1896.
55 D. E. Couture-Rigert, P. J. Sirois and E. A. Moffatt, *Stud. Conserv.*, 2012, **57**, 142–163.
56 S. Barreca, M. Bruno, L. Oddo and S. Orecchio, *Nat. Prod. Res.*, 2019, **33**, 947–955.
57 V. M. Pozhidaev, V. M. Retivov, A. V. Kamaev, S. K. Belus, A. S. Nartov, V. A. Rastorguev, I. V. Borodin, E. Y. Tereschenko, R. A. Sandu, E. B. Yatsishina and M. V. Kovalchuk, *Heritage Sci.*, 2019, **7**, 90.
58 L. Kubick and J. Giaccai, *AIC Objects Specialty Group Postprints*, 2012, vol. 19, pp. 45–69.
59 G. D'Ercoli, M. Marabelli, V. Santin, A. Buccolieri, G. Buccolieri, A. Castellano and G. Palamà, in *9th International Conference on NDT of Art*, Jerusalem, 2008.
60 I. M. Marcelli and M. Mercalli, in *9th International Conference on NDT of Art*, Jerusalem, 2008.
61 J. Wolfe, R. Grayburn, H. Khanjian, A. Heginbotham and A. Phenix, in *ICOM-CC 18th Triennial Conference*, Copenhagen, 2017.
62 E. Risser, D. Saunders and J. P. G. Museum, The restoration of ancient bronzes: Naples and beyond, 2013.
63 U. Knutinen and A. Norman, in *15th World Conference on Nondestructive Testing*, Rome, 2000.
64 N. Swartz and T. L. Clare, *J. Am. Inst. Conserv.*, 2015, **54**, 181–201.
65 C. Lim, *Collections Care: Staying Relevant in Changing Times, ASEAN & Beyond*, Singapore, 2019.
66 S. Kezic, J. Kruse and I. Jakasa, *Review of dermal effects and uptake of petroleum hydrocarbons*, 2010.
67 S. Parasuraman, W. Ping, P. Raj, J. Sujithra, B. Syamittra, W. Yeng, S. Dhanaraj and S. Muralidharan, *J. Basic Clin. Pharm.*, 2014, **5**, 89.
68 M. A. Amoruso, J. F. Gamble, R. H. McKee, A. M. Rohde and A. Jaques, *Int. J. Toxicol.*, 2008, **27**, 97–165.
69 S. L. Edgar, *Pigm. Resin Technol.*, 1982, **11**, 13–18.
70 A. Bhardwaj, K. Srinivas and R. Chaudhary, *Natl. Acad. Sci. Lett.*, 2024, DOI: **10.1007/s40009-024-01400-9**.
71 M. Díaz de Los Ríos and E. Hernández Ramos, *SN Appl. Sci.*, 2020, **2**, 676.
72 C. M. Hansen, *Hansen Solubility Parameters: A User's Handbook*, CRC Press, Boca Raton, 2nd edn, 2007.
73 J. P. Teas, *J. Paint Technol.*, 1968, **40**, 19–25.
74 C. M. Hansen, *Hansen solubility parameters: a user's handbook*, CRC Press, 2000.
75 International Commission on Illumination, Colorimetry, Commission Internationale de l'Eclairage, 2004.
76 T. T. Duncan, E. P. Vicenzi, T. Lam and S. A. Brogdon-Grantham, *J. Am. Inst. Conserv.*, 2023, **62**, 152–167.
77 P. Yu, *Detect Structural Features of Asymmetric and Symmetric CH_2 and CH_3 Functional Groups and Their Ratio of Biopolymers Within Intact Tissue in Complex Plant System Using Synchrotron FTIRM and DRIFT Molecular Spectroscopy*.
78 J. F. Su, Z. Huang, X. Y. Yuan, X. Y. Wang and M. Li, *Carbohydr. Polym.*, 2010, **79**, 145–153.
79 B. A. S C Lawrence, *Trans. Faraday Soc.*, 1938, **44**, 660–677.
80 J. W. Mcbain and W. L. Mcclatchie, *J. Phys. Chem.*, 1932, **36**, 2567–2574.
81 S. S. Sagiri, V. K. Singh, K. Pal, I. Banerjee and P. Basak, *Mater. Sci. Eng., C*, 2015, **48**, 688–699.
82 F. Fratini, G. Cilia, B. Turchi and A. Felicioli, *Asian Pac. J. Trop. Med.*, 2016, **9**, 839–843.
83 R. Sedev, *Curr. Opin. Colloid Interface Sci.*, 2011, **16**, 310–316.
84 T. T. Chau, W. J. Bruckard, P. T. L. Koh and A. V. Nguyen, *Adv. Colloid Interface Sci.*, 2009, **150**, 106–115.
85 W. S. Mokrzycki and M. Tatol, *Colour Difference ΔE – A Survey*, Olsztyn, 2012.
86 D. A. G. Martínez, E. V. Santiago and S. H. López, *Polymers*, 2021, **13**, 852.
87 A. M. Hassan, A. M. Mazrouaa, M. A. Youssif, R. M. A. Shahba and M. A. Youssif, *Int. J. Org. Chem.*, 2013, **03**, 71–80.
88 X. Ma, V. Beltran, G. Ramer, G. Pavlidis, D. Y. Parkinson, M. Thoury, T. Meldrum, A. Centrone and B. H. Berrie, *Angew. Chem., Int. Ed.*, 2019, **58**, 11652–11656.
89 J. H. Hildebrand and R. L. Scott, *Regular solutions*, Prentice-Hall, Englewood Cliffs, N.J., 1962.
90 P. J. Flory, *Principles of Polymer Chemistry*, Cornell University Press, New York, 1953.
91 L. Ivanovszky, *Waxes: Colloidal Properties and Systems*, 1962, vol. 58.
92 M. Aqil, B. Abderrahim, E. Abderrahman, A. Mohamed, T. Fatima, T. Abdesselam and O. Krim, *World J. Environ. Eng.*, 2015, **3**, 95–110.